Science Advances

AAAS

Supplementary Materials for

Highly efficient hot electron harvesting from graphene before electron-hole thermalization

Yuzhong Chen, Yujie Li, Yida Zhao, Hongzhi Zhou, Haiming Zhu*

*Corresponding author. Email: hmzhu@zju.edu.cn

This PDF file includes:

Section S1. Determining doping level and chemical potential in graphene
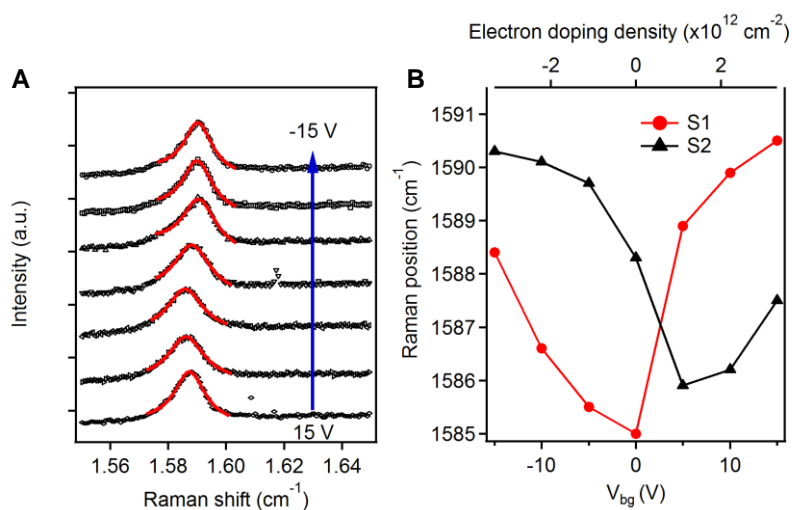

Fig. S1. Determining doping level and chemical potential in graphene. (**A**) Raman spectra of Gr/WS₂ heterostructure sample at different back gating voltages showing region of graphene G peak. (**B**) The position of graphene Raman G peak for two Gr/WS₂ heterostructure samples as a function of back gating voltages.

We determined the graphene doping level in heterostructure based on the Raman peak of graphene which is very sensitive to the carrier doping.(*45, 46*) Using Gr/WS₂ heterostructure samples with graphene in direct contact with pre-patterned gold electrode on a SiO_2(100 nm)/Si substrate, we measured the graphene Raman G peak as function back gating voltage (V_{bg}) in the heterostructure area. The Raman spectra are shown in fig. S1A, from where we extract the G peak position. The G peak positions as a function of back gating for two different samples are shown in fig. S1B. Obviously, they show a dip around 0~5 V, corresponding to charge neutral graphene.(*45, 46*) Therefore, graphene in heterostructure is slightly P-doped. Based on the capacitance, we calculated the doping density $\leq 10^{12}$ cm^{-2}. Given the density of states of graphene, we can calculate the chemical potential of ~ 130 meV below Dirac point.

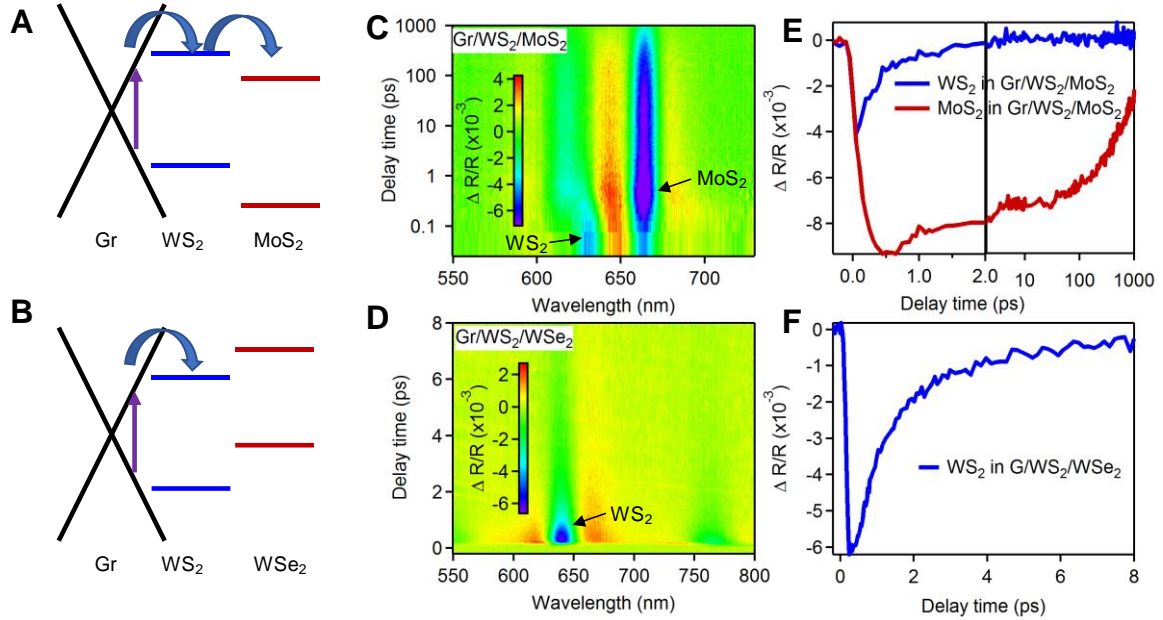## Section S2. Selective carrier extraction from Gr/WS$_2$ heterostructures and charge recombination retardation

Fig. S2. Selective carrier extraction and charge recombination retardation. Scheme showing the band alignment of (**A**) Gr/WS$_2$/MoS$_2$ and (**B**) Gr/WS$_2$/WSe$_2$ heterostructures, where electron (hole) in WS$_2$ can further transfer to MoS$_2$ (WSe$_2$). TR spectra of (**C**) Gr/WS$_2$/MoS$_2$ and (**D**) Gr/WS$_2$/WSe$_2$ heterostructures under 900nm (1.37 eV) excitation where we only excite graphene, showing strong TA signal in MoS$_2$ but not in WSe$_2$. TR kinetics of WS$_2$ in (**E**) Gr/WS$_2$/MoS$_2$ and (**F**) Gr/WS$_2$/WSe$_2$ heterostructures. We also show MoS$_2$ kinetics for comparison.

We performed selective carrier extraction from Gr/WS$_2$ heterostructure to unambiguously confirm electron injection in to WS$_2$ instead of hole and to retard charge recombination. We added a third carrier extraction layer, MoS$_2$ and WSe$_2$, next to WS$_2$ in GR/WS$_2$ heterostructure. According to the band alignment(*44*) as shown in fig. S2A and 2B, MoS$_2$ will accept electron from WS$_2$ but not hole while WSe$_2$ will extract hole from WS$_2$ but not electron. Once electron or hole transfer to third layer with the counter-carrier in graphene, electron and hole are spatially separated and recombine in a much longer timescale, compared to Gr/WS$_2$.

The TR spectra of Gr/WS₂/MoS₂ and Gr/WS₂/WSe₂ heterostructures are shown in C and D, respectively. In Gr/WS₂/MoS₂, photoexcitation initially leads to TR bleach of WS₂ A exciton which quickly decays in 1ps, accompanying which a prominent bleach of MoS₂ A exciton forms. The MoS₂ bleach decays in hundreds of ps (with a half-life time ~ 500 ps). The interconversion process between WS₂ and MoS₂ and long-lived electron in MoS₂ clearly indicates hot electron transfer from graphene to WS₂ and then to MoS₂. In Gr/WS₂/WSe₂ heterostructure, photoexcitation leads to prominent bleach of WS₂ A exciton, which decays just as in Gr/WS₂ heterostructure without any long-lived signal left. Unlike Gr/WS₂/MoS₂, Gr/WS₂/WSe₂ only shows a very weak peak at WSe₂ A exciton position which rises and decays in the same way as electron in WS₂. This signal is due to electron in WS₂, which modulate the A exciton transition in WSe₂ through dielectric effect. These results clearly show electron transfer from graphene to WS₂ with negligible hole transfer in Gr/WS₂ heterostructure.

Section S3. QY calibration using WSe₂/WS₂ heterostructure and direct high-energy excitation
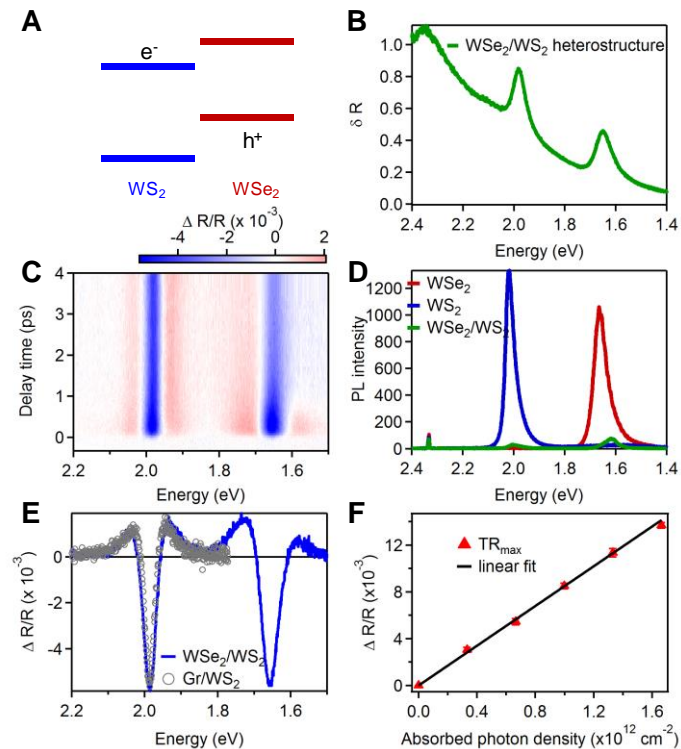
Fig. S3. CT in WSe₂/WS₂ heterostructure. (**A**) Type II band alignment of WSe$_2$/WS$_2$ heterostructure with electron in WS$_2$ and hole in WSe$_2$. (**B**) Reflectance contrast spectrum of WSe$_2$/WS$_2$ heterostructure (**C**) Color plot of TR spectra of WSe$_2$/WS$_2$ monolayer/monolayer heterostructures at 550 nm (2.25 eV) excitation, showing clearly A exciton bleach from both WS$_2$ and WSe$_2$ due to electron in WS$_2$ and hole in WSe$_2$. (**D**) PL spectra of WSe$_2$, WS$_2$ monolayers and WSe$_2$/WS$_2$ heterostructure. (**E**) A representative TR spectrum of WSe$_2$/WS$_2$ heterostructure at 0.5 ps delay time. Also shown is the TR spectrum of Gr/WS$_2$, which matches very well with that of WSe$_2$/WS$_2$ heterostructure at WS$_2$ A exciton position. (**F**) TR peak amplitude (TR$_{max}$) of WS$_2$ A exciton bleach in WS$_2$/WSe$_2$ heterostructure as a function of absorbed photon density.

We prepared a WSe$_2$/WS$_2$ heterostructure sample on SiO$_2$ using exfoliation and stacking method. WSe$_2$/WS$_2$ heterostructure is known to have type II band alignment with electron in WS$_2$ and hole in WSe$_2$ (fig. S3A) and the interfacial charge transfer between them occurs in ultrafast (< 50 fs) timescale.(*39, 44, 47-48*) fig. S3B shows the reflectance contrast spectrum of WSe$_2$/WS$_2$ heterostructure sample on SiO$_2$, where the peaks ~ 2 eV and 1.75 eV correspond to WS$_2$ and WSe$_2$ A exciton bleach, respectively. The PL spectra of monolayers and heterostructure are shown in fig. S3D. The PL from WS$_2$ and WSe$_2$ are almost completely quenched in heterostructure, consistent with previous studies showing ultrafast interfacial charge transfer.(*39, 44, 47-48*)

The color plot of TR spectra of WSe$_2$/WS$_2$ heterostructure is shown in fig. S3C under 550 nm (2.25 eV) excitation. We observe distinct bleach peaks at ~ 2.0 and 1.75 eV, corresponding to WS$_2$ and WSe$_2$ A exciton peaks, respectively. Given the type II band alignment, these A exciton bleach peaks are due to electron and hole occupation in each layer. We compared a representative TR spectrum of WSe$_2$/WS$_2$ to that of Gr/WS$_2$ (fig. S3E). The near identical TR spectra at WS$_2$ A exciton bleach suggest electron transfer to WS$_2$, which was further confirmed in selective carrier extraction study above (S3). We take peak amplitude of TR kinetics (TR$_{max}$) at WS$_2$ A exciton

bleach and plot the TR_{max} as a function of absorbed photon density. Obviously, the electron occupation induced TR signal at WS_2 A exciton peak increase linearly with absorbed photon density in the small signal regime ($\Delta R/R < 0.01$). Therefore, in our TR study we maintain TR signal in this regime to reflect the electron population in WS_2.

Furthermore, we can calibrate electron injection QY in Gr/WS_2 using TR signal from WSe_2/WS_2 heterostructure. In WSe_2/WS_2, given the near-complete quenching of PL and ultrafast interfacial electron transfer (orders of magnitude faster than intrinsic decay lifetime in each monolayer), the charge separation yield can be considered as unity. Therefore, all absorbed photons contribute to electrons in WS_2 in WSe_2/WS_2 heterostructure. That is, the slope of TR_{max} vs N_{photon} plot of WSe_2/WS_2 heterostructure corresponds to a QY of 100%. Using this as a reference and the slopes of TR_{max} vs N_{photon} plot in Gr/WS_2, we can calculate the electron injection QY in Gr/WS_2 heterostructure at all excitation photon energies as shown in fig. S3D in main text.
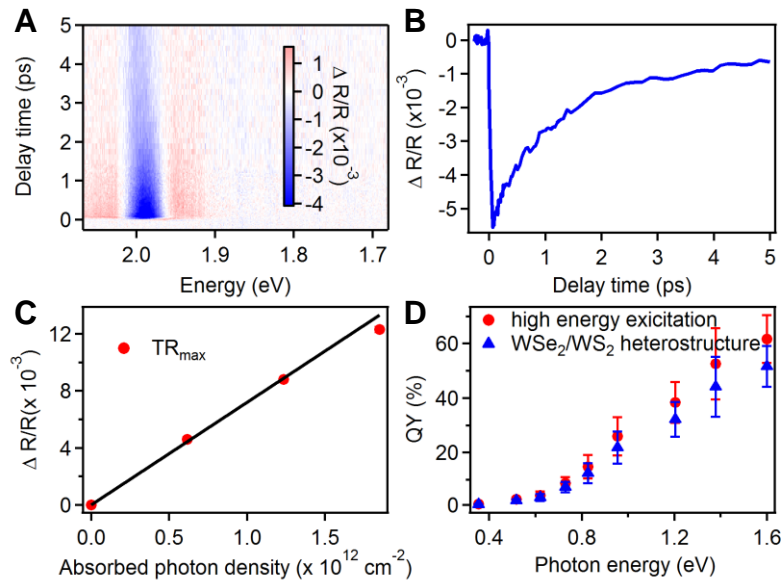
Fig. S4. TR measurements of Gr/WS_2 under above-gap excitation. (**A**) Color plot of TR spectra of Gr/WS_2 under 515 nm (2.41 eV) excitation, showing A exciton bleach of WS_2. (**B**) TR kinetics of WS_2 A exciton bleach (**C**) peak amplitude of TR kinetics at different absorbed photon density (**D**) QY of Gr/WS_2 under different photon energy using two different calibration method: direct high energy excitation *vs* WSe_2/WS_2 heterostructure.

We also calibrated QY by directly exciting the same Gr/WS$_2$ sample with a high energy photon (above bandgap of WS$_2$). Here we choose 515 nm (2.41 eV) excitation with major absorption from WS$_2$. The color plot of TR spectra of GR/WS$_2$ is shown in fig. S4A and the TR kinetics of WS$_2$ exciton bleach is shown in fig. S4B. The peak amplitude of TR kinetics (TR$_{max}$) right after 515 nm excitation is shown in fig. S4C, which shows a linear relationship in small signal regime. Under 515 nm excitation, most (~ 78%) of photon absorption is contributed directly by WS$_2$ itself. Therefore, the slope of *TR$_{max}$ vs N$_{photon}$* plot can be approximated to correspond to 100% QY. Using this as reference and the slopes of *TR$_{max}$* vs *N$_{photon}$* plot in Gr/WS$_2$ at sub-bandgap excitation, we can calculate the electron injection QY in Gr/WS$_2$ heterostructure at all excitation energies.

Hot electron injection QY determined by these two different methods are shown in fig. S4D and they are differed by a relative value of ~ 10 %. We report averaged values between them in main text.
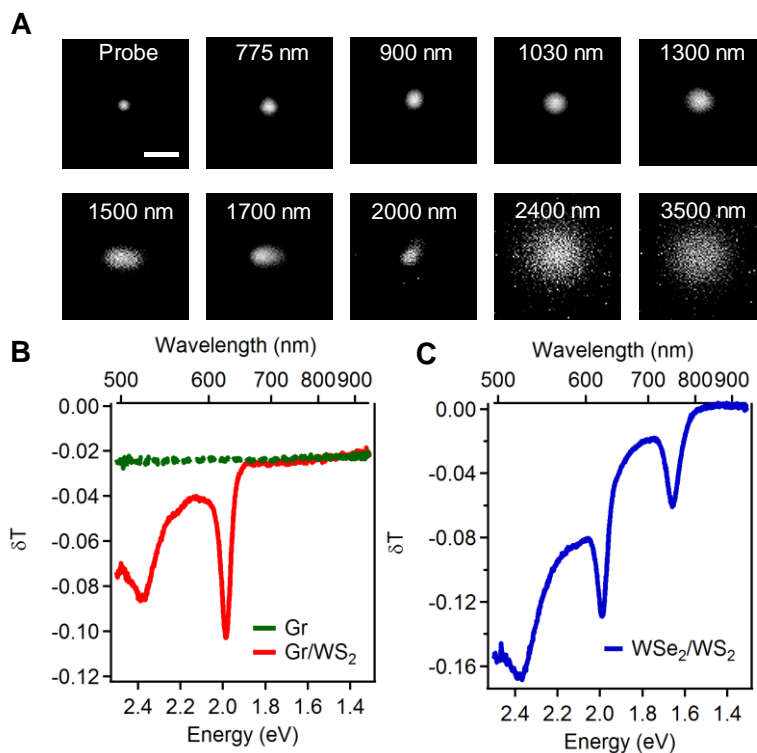
Section S4. Absorbed photon density calculation

Fig. S5. Beam profile and absorption properties of heterostructures. (**A**) Optical image of pump and probe beams on sample, from which we can calculate precisely the photon density in the probe area. Scale bar: 5μm. (**B**) and (**C**): Transmittance contrast (δT) of Gr/WS$_2$ and WSe$_2$/WS$_2$ heterostructure samples, respectively, for calculating absorption percentage as described.

In this study, it is critical to precisely determine the absorbed photon density in the probe area at different excitation photon energies. Thanks to the microscopic transient reflectance setup, we can take optical images of pump and probe beams directly when they are overlapped on samples. The optical images are shown in fig. S5A. The probe beam is ~ 0.6 μm and the pump beam is always larger enough to cover probe area. The exact fraction of pump power falling into probe are can be determined accurately based on the pixel intensities on optical images directly (= pump intensity in probe area/total pump intensity on image). Together with the probe area, we can calculate the pump photon density precisely.

For sub-bandgap excitation on graphene, we directly take absorption constant (2.3 %) of graphene to calculate absorbed photon density. For above gap excitation (WSe$_2$/WS$_2$ and Gr/WS$_2$ heterostructures in SI4 for QY calibration), we must calculate the absorption considering both reflectance and transmittance effect. The reflectance contrast is calculated as $\delta R = (I_s^R - I_0^R)/I_0^R$, where I_s^R and I_0^R are the reflected light intensity from sample and substrate (SiO$_2$), respectively. δR of Gr/WS$_2$ and WSe$_2$/WS$_2$ heterostructures are shown in Fig. 2E of main text and fig. S3B. The transmittance contrast (δT) is calculated as $\delta T = (I_s^T - I_0^T)/I_0^T$, where I_s^T and I_0^T are the transmitted light intensity from sample and substrate (SiO$_2$), respectively. δT of Gr/WS$_2$ and WSe$_2$/WS$_2$ heterostructures are shown fig. S5B and S5D. The absorption percentage (Abs) was calculated with δR, δT and the absorption (=0) and reflection (3.5% with refractive index $n_s = 1.457$) of SiO$_2$ by $Abs = -0.035\delta_R - 0.965\delta_T$. With these, we can calculate the absorption of Gr/WS$_2$ and WSe$_2$/WS$_2$ heterostructures at excitation wavelength. Then the absorbed photon density can be calculated by multiplying pump photon density with absorption percentage.

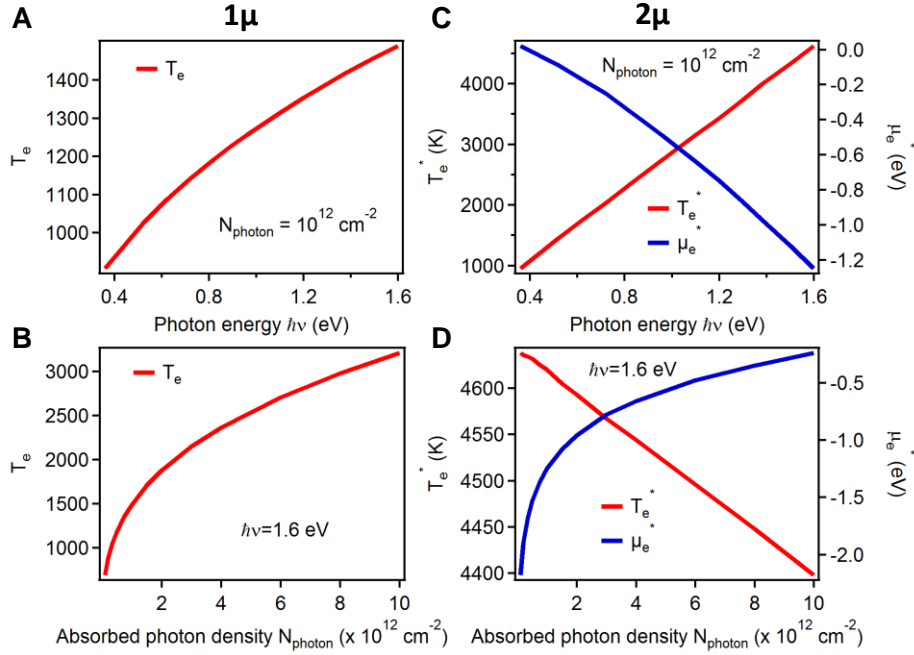## Section S5. Calculation with 1μPTE model and 2μPTE model

Fig. S6. Calculated carrier temperature and chemical potential with different models. (left panel) calculated electron temperature according to 1μ model. (**A**): electron temperature as a function of photon energy at a fixed photon density (10^{12} cm^{-2}) (**B**): electron temperature as a function of absorbed photon density at a fixed photon energy (1.6 eV). (right panel) calculated electron temperature according to 2μ model. (**C**): electron temperature and chemical potential as a function of photon energy at a fixed photon density (10^{12} cm^{-2}) (**D**): electron temperature and chemical potential as a function of absorbed photon density at a fixed photon energy (1.6 eV)

In 1μPTE model after thermalization, the whole electronic system reaches a thermal equilibrium described by FD distribution with one well-defined T_e and μ (we take $\mu = 0$ for charge neutral graphene here)

$$f_e(E) = \frac{1}{\exp(\frac{E}{k_B T_e})+1} \tag{S1}$$

Considering energy conservation at equilibrium

$$\int_0^\infty dE f_e(E) g(E) E - \int_{-\infty}^0 dE (1 - f_e(E)) g(E) E = \eta N_{photon} \hbar \nu \qquad (S2)$$

$g(E)$ is the density of states of graphene and η is the fraction of excitation energy that goes to electronic system and we take the value of 70% accounting the phonon emission lose during thermalization process.(26) In this model, only energy conservation is considered and electron population is no longer conserved due to interband scattering (e.g. Auger and invers Auger process) which is also not required in the calculation process. From equation S1 and S2, we can calculate electron temperature (T_e) for a certain N_{photon} and $\hbar \nu$. Then the carrier distribution is solely determined by S1. As shown in fig. S6A and S6B, electron temperature increases with both N_{photon} and $\hbar \nu$ sub-linearly in 1μPTE model. The hot electron injection QY is calculated as the fraction of electrons above barrier height (φ_B)

$$QY = \frac{\int_{\varphi_B}^\infty dE f_e(E) g(E)}{N_{photon}} \qquad (S3)$$

In 2μPTE model, electron and hole establish separate thermal equilibrium distributions with distinct temperatures ($T_{e(h)}^*$) and chemical potentials ($\mu_{e(h)}^*$) in each band

$$f_{e(h)}(\varepsilon) = \frac{1}{\exp(\frac{\varepsilon - \mu_{e(h)}^*}{k_B T_{e(h)}^*}) + 1} \qquad (S4)$$

Given the ultrafast intraband scattering process, both energies (half into each band) and carriers are approximated to be conserved in our model

$$\int_0^\infty dE f_e(E) DOS(E) E = \frac{1}{2} N_{photon} \hbar \nu \qquad (S5)$$

$$\int_0^\infty dE f_e(E) DOS(E) = N_{photon} \qquad (S6)$$

From equation S4, S5 and S6, we can calculate both electron temperature (T_e^*) and chemical potential (μ_e^*) for a certain N_{photon} and $\hbar\nu$. As shown in fig. S6C, with increasing photon energy $\hbar\nu$, electron temperature increases linearly, and chemical potential moves down monotonically to be more negative (below Dirac point). Interestingly, at a fixed photon energy, with increasing absorbed photon density, electron temperature decreases, and chemical potential shifts up to accommodate more electrons in conduction band (fig. S6D). The hot electron injection QY can be calculated as the fraction of electrons above barrier height (φ_B) using equation S3.
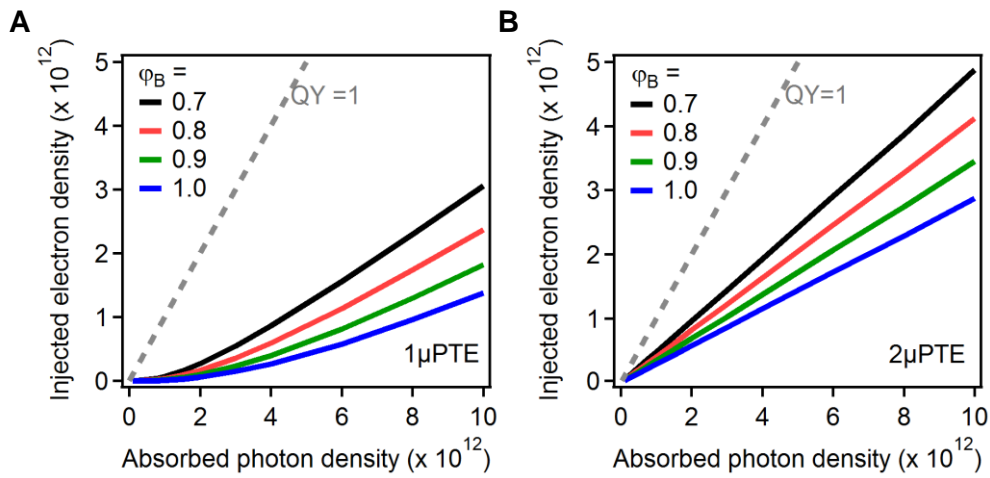

Fig. S7. Calculated injection electron density. Injected electron density vs absorbed photon density for different barrier height using (**A**) 1μPTE model and (**B**) 2μPTE model. Excitation photon energy was chosen to be 1.6 eV. Also shown in gray dashed line is where injected electron density equals to absorbed photon density, i.e. QY = 100%.

In fig. S7, we compare the injected electron density *vs* absorbed photon densities for these two different models. We also varied the barrier height between 0.7 and 1 eV. Also shown in gray dashed line is where injected electron density equals to absorbed photon density, i.e. QY = 100%. Obviously, injected electron density shows superlinear dependence on absorbed photon density in 1μPTE model but linear behavior in 2μPTE model. The injection QY in 2μPTE model is significantly higher than 1μPTE model, especially at small absorbed photon density.

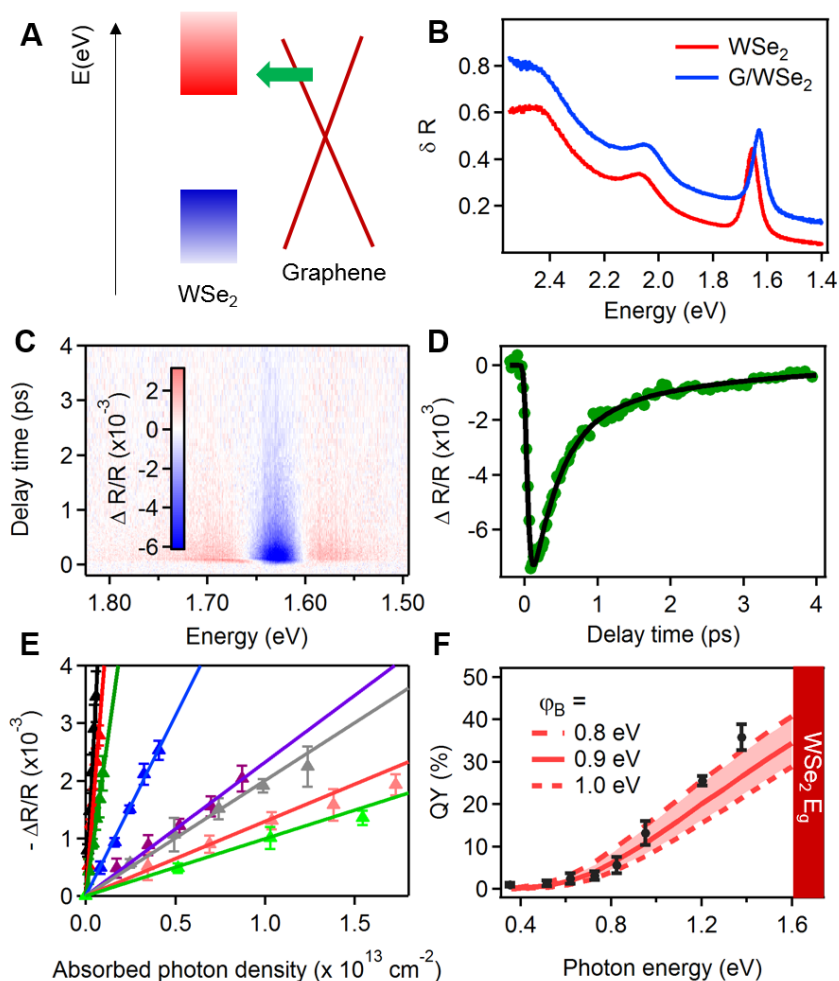## Section S6. Hot electron transfer from photoexcited graphene to WSe$_2$

Fig. S8. Hot electron transfer from photoexcited graphene to WSe$_2$. (**A**) Scheme showing the band alignment between WSe$_2$ and graphene and photoexcited electron transfer from graphene to WSe$_2$. (**B**) Reflectance contrast spectra of WSe$_2$ monolayer and Gr/WSe$_2$ heterostructure. (**C**) Color plot of TR spectra of Gr/WSe$_2$ heterostructure under 1.3 eV below gap excitation. (**D**) TR kinetics of WSe$_2$ A exciton bleach and exponential fitting (**E**) Peak amplitude of TR signal for eight different photon energies as a function of absorbed photon densities, showing a clear linear dependence. Solid lines are linear fits. From left to right: 1.4, 1.2, 0.95, 0.83, 0.73, 0.62, 0.52, 0.35 eV. (**F**) Experimentally determined QY (black circles) of hot electron injection as a function of photon energies showing continuous increasement with photon energy. Lines are predictions based on 2μPTE with different barrier heights (0.8, 0.9, 1.0 eV).

We also prepared Gr/WSe$_2$ heterostructure sample with band alignment shown in fig. S8A. The reflectance contrast spectra of WSe$_2$ monolayer and Gr/WSe$_2$ heterostructure are shown in fig. S8B. WSe$_2$ monolayer shows an A exciton peak at ~ 1.75 eV, which is redshifted and broadened in Gr/WSe$_2$ heterostructure. We excited the heterostructure sample with different photon energies below WSe$_2$ bandgap. The color plot of TR spectra of Gr/WSe$_2$ heterostructure under 1.3 eV is shown in fig. S8C. A clear bleach peak at WSe$_2$ A exciton peak position can be observed, indicating electron transfer from photoexcited graphene to WSe$_2$. Previous photocurrent measurement confirms electron injection to WSe$_2$.(*26*) The TR kinetics at WSe$_2$ A exciton peak position is shown in fig. S8D. Fitting the kinetics yields a rising time of 40 ± 5 fs and a biexponential decay with a half-life time of ~ 0.55 ps, which corresponds to hot electron transfer from graphene to WSe$_2$ and subsequent back electron transfer to graphene, respectively.

We varied the excitation photon energy and density and performed TR measurement. The peak amplitude values (TR$_{max}$) of TR kinetics at different photon energies were plot a function of absorbed photon density in fig. S8E. Obviously, TR$_{max}$ scales linearly with absorbed photon density, except the onset of sublinear deviation at high absorbed photon density of low photon energy, as in Gr/WS$_2$ heterostructure. From the slope of linear fitting, we can calculate the electron injection QY at different photon energies and the result is shown in fig. S8F. Also shown in fig. S8F is the calculated QY using 2μPTE model with three different barrier heights (0.8, 0.9, 1.0 eV) and experimental values fall into the calculated range.
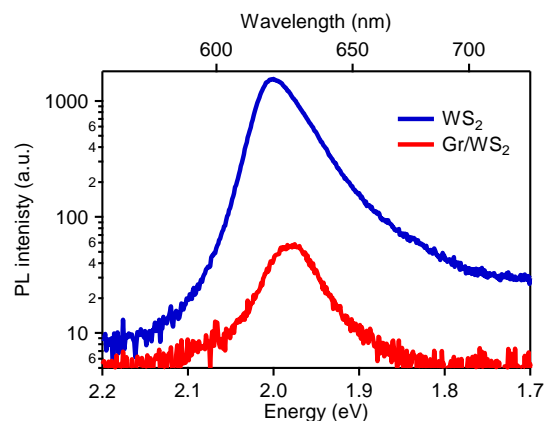
Section S7. Additional figures

Fig. S9. PL spectra of WS$_2$ monolayer and Gr/WS$_2$ heterostructure. The
photoluminescence of WS$_2$ is quenched by more than one order of magnitude in
heterostructure. The trion feature in intrinsically n-doped WS$_2$ monolayer disappeared
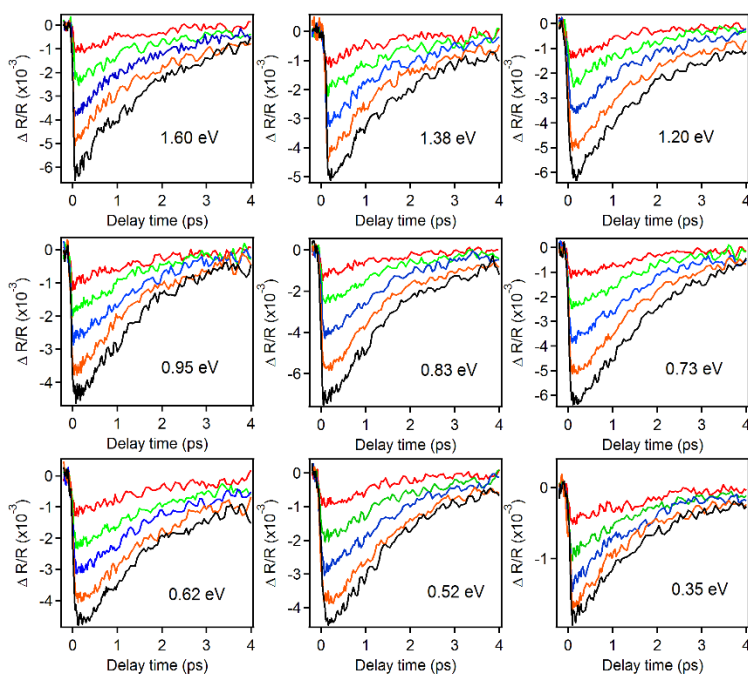in heterostructure, suggesting static electron flow from unintentional n-doped WS$_2$ to
p-doped Gr.

**Fig. S10. All TR kinetics of Gr/WS$_2$ heterostructure at WS$_2$ A exciton bleach, at
different excitation photon energies and densities.** from which we extracted the
peak amplitude TR$_{max}$. The photon energies are labeled in Figures above and absorbed
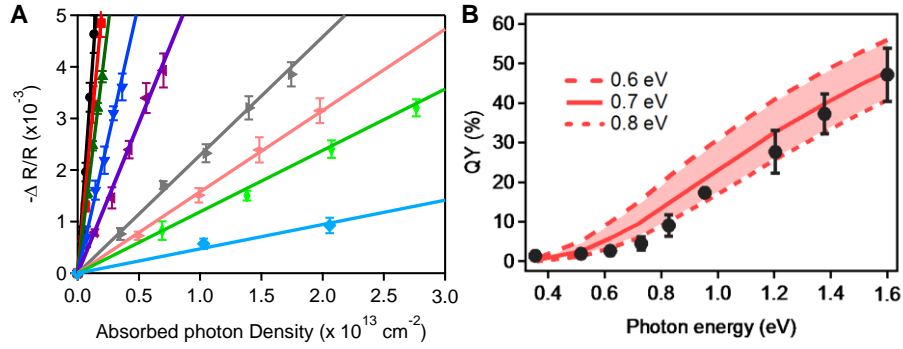photon densities are plotted in Fig. 3C in main text.

Fig. S11. TR results from another Gr/WS₂ sample. (**A**) Peak amplitude of TR signal for nine different photon energies as a function of absorbed photon density, showing a clear linear dependence. Solid lines are linear fits. From left to right: 1.6, 1.4, 1.2, 0.95, 0.83, 0.73, 0.62, 0.52, 0.35 eV. (**B**) Experimentally determined QY (black circles) of hot electron transfer as a function of photon energies showing continuous increasement with photon energy. Lines are predictions based on 2μPTE with different barrier heights (0.6, 0.7, 0.8 eV).
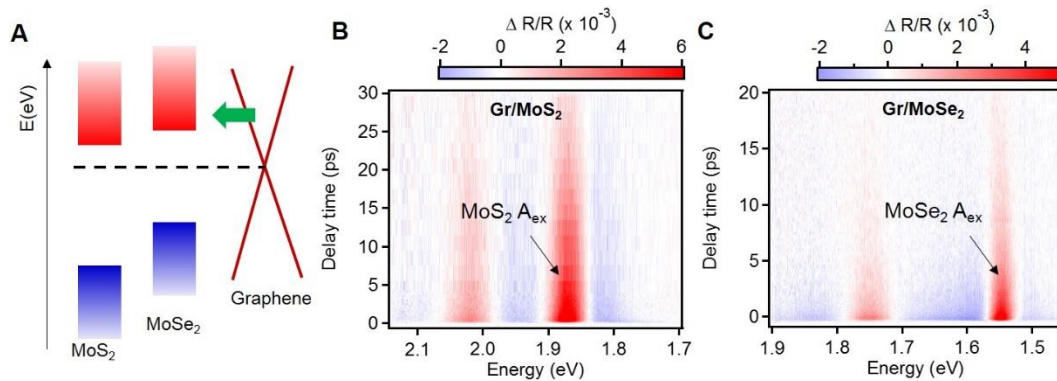

Fig. S12. TR spectra of Gr/MoS₂ and Gr/MoSe₂ heterostructures. (**A**) Scheme showing band alignment between MoS₂, MoSe₂ and graphene and electron transfer from photoexcited graphene to MoS₂ and MoSe₂. Color plot of TR spectra of Gr/MoS₂ (**B**) and Gr/MoSe₂ (**C**) heterostructure under 1.3 eV below gap excitation, showing clearly A exciton bleach of MoS₂ and MoSe₂ due to electron transfer from photoexcited graphene.